10th International Conference on Fracture Mechanics of Concrete and Concrete Structures
FraMCoS-X
G. Pijaudier-Cabot, P. Grassl and C. La Borderie (Eds)
https://doi.org/10.21012/FC10.232582

EVALUATION OF INTERFACE FRACTURE IN MODEL CONCRETE

TAISUKE NATSUME[*], SONOKO ICHIMARU[†], HIDEKI NAITO[††] AND JOHN E. BOLANDER[†††]

[*] Dept. of Civil and Environmenrtal Engineering, Tohoku University
6-6-06 Aramaki Aza Aoba, Aoba-ku, Sendai, Miyagi, Japan
e-mail: taisuke.natsume.p4@dc.tohoku.ac.jp

[†] Dept. of Civil and Environmental Engineering, University of California, Davis
One Shields Avenue, Davis, California, U.S.A.
e-mail: sichimaru@ucdavis.edu

[††] Dept. of Civil and Environmenrtal Engineering, Tohoku University
6-6-06 Aramaki Aza Aoba, Aoba-ku, Sendai, Miyagi, Japan
e-mail: hideki.naito.c2@tohoku.ac.jp

[†††] Dept. of Civil and Environmental Engineering, University of California, Davis
One Shields Avenue, Davis, California, U.S.A.
e-mail: jebolander@ucdavis.edu

Key words: Composite material, Interface fracture, Damage detection, Vibration

Abstract: The effectiveness of forced vibration testing to detect interface fracture within model concrete is examined. Model concrete cylinders containing spherical glass aggregates or voids were cast. Quasi-static load was applied to induce interface fracture between the aggregates and mortar. Resonant frequency was measured from longitudinal standing vibration of the cylinders. Results indicated that the resonant frequency decreased as the amount of voids or load increased. Wave propagation analyses were then used to interpret the experimental results. The calculations indicated that the waves diffracted around the voids during standing vibration, and the diffracted waves decreased the resonant frequency. A similar result was also shown in the cylinders containing interface fractures, since they act as discontinuities along the aggregate-mortar boundaries. Furthermore, the damage conditions within the composite material were also evaluated using these testing and calculation methods. In the load tests, internal cracks were relatively stable in the plain mortar cylinders in the vicinity of maximum load, whereas internal damage of the cylinders containing the glass aggregates developed quickly. The effectiveness of forced vibration testing was demonstrated not only in identifying interface fracture within composite materials, but also in measuring the degree of resulting damage.

1 INTRODUCTION

For most cement-based composites and structures, their performance depends greatly on the properties of interfaces between the constituent materials. Interfacial fracture can severely degrade performance with respect to strength, ductility, and durability [1]. Therefore, it is important to detect interface fracture and understand its growth mechanisms for designing new composite materials, improving their performance, and inspecting and evaluating aging composite structures.

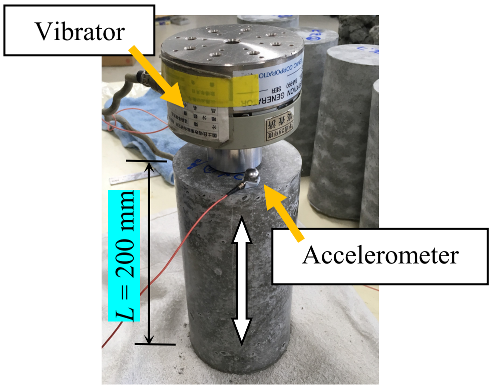

Figure 1: Forced vibration test on a mortar cylinder.

Numerical simulation has been widely used for investigating interface fracture within composite materials and structures [2, 3]. Additionally, nondestructive testing methods can provide information on internal damage conditions. The measured data can also be useful for determining parameter values for the simulations. However, most of the standard testing methods (based on, e.g., radar [4], ultrasonic waves [5-8], and impact echoes [9]) typically face difficulties in evaluating internal damage conditions, including interface fracture. These waves reflect and scatter on the interfaces and other heterogeneous features near the surface of structures.

In this study, a portable vibrator was utilized to detect the interface fracture within model concrete cylinders containing spherical glass aggregates. The vibrator excites longitudinal standing vibration of the cylinders, as shown in **Figure 1**. The wavelength is $2L$ during the standing vibration, where L is the cylinder length. When the size of interface fracture is smaller than the wavelength, $2L$, the waves diffract around the fractured area and decrease the resonant frequency [10]. Therefore, it is expected that the degree of interface fracture can be evaluated from the decrease of the resonant frequency.

The objective of this study is to assess the ability of the test method to detect interface fracture and evaluate the internal damage condition. Mortar cylinders containing spherical glass aggregates or voids were cast. Quasi-static load was then applied to cylinders to induce interface fracture between the aggregates and mortar matrix. The cylinders were then excited dynamically to produce standing vibration, from which resonant frequency was measured. Additionally, wave propagation analyses using a finite difference time domain (FDTD) method were used to interpret the experimental results.

Table 1: Cylinder specimens containing the aggregates or voids.

Spec-imen	Inclusion type	Number of aggregates or voids	Volume ratio
N0	None	0	0%
BF	Glass aggregates	108	Aggregates: 55%
V0	None	0	0%
V10	Spherical voids	19	Voids: 10%
V20		38	Voids: 20%
V30		58	Voids: 30%
V40		77	Voids: 40%

2 FORCED VIBRATION TESTS AND ANALYSES

2.1 Forced vibration tests

2.1.1 Test specimens

The test parameters are indicated in **Table 1**. Three replicate specimens were produced for each specimen type. The cylinders had a diameter of 100 mm and length of 200 mm. A mixture of non-AE mortar was used: water at a weight per cubic meter W = 280 kg/m^3, early strength cement C = 467 kg/m^3, and fine aggregate S = 1401 kg/m^3. The material properties of the mortar were obtained from testing the plain specimen N0: the speed of sound c_m = 3388 m/s, the mass density ρ_m = 2030 kg/m^3, and the dynamic elastic modulus E_m = 23,300 MPa.

Specimen BF contained glass aggregates with a diameter of 25 mm, as shown in **Figures 2** and **3**. These aggregates were then packed into the cylinder molds, which were then filled with the mortar on a shaking table for 3 minutes. The mass density of the glass

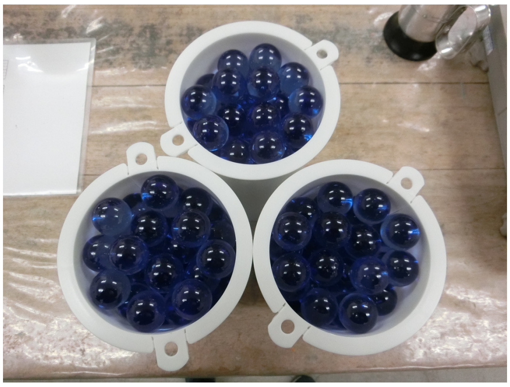

Figure 2: Glass aggregates packed into molds.

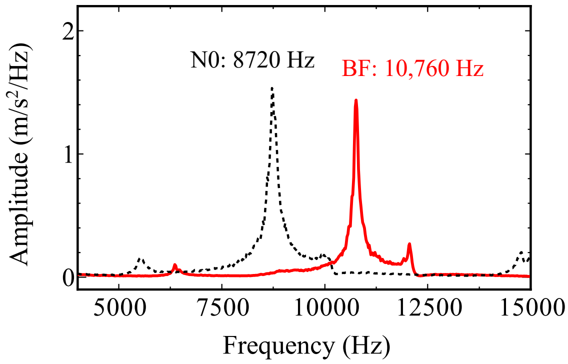

Figure 4: Frequency responses of specimens N0 and BF.

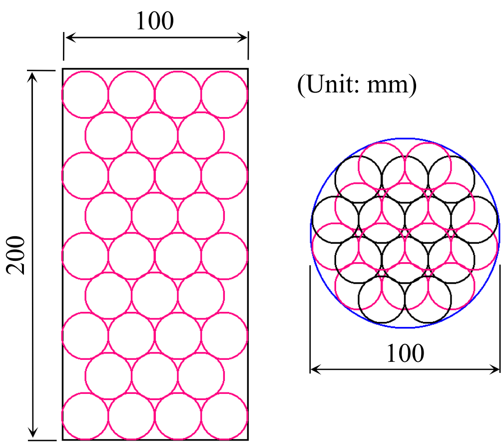

Figure 3: Arrangement of the aggregates.

was measured as ρ_g = 2470 kg/m^3. The speed of sound c_g and dynamic elastic modulus E_g of the glass aggregates were estimated as 5397 m/s and 71,300 MPa, respectively, as later given in Eqs. (1), (2).

Specimen V0 did not contain voids, whereas specimens V10 to V40 contained foam spheres (voids) with a diameter of 25 mm. These voids were mixed and distributed while casting the mortar into a mold. The volumetric void ratio of specimens V10 to V40 was changed from 10% to 40%, as shown in **Table 1**. For these void specimens, the mortar material properties were obtained from testing specimen V0: the speed of sound c_m = 3440 m/s, the mass density ρ_m = 2060 kg/m^3, and the dynamic elastic modulus E_m = 24,400 MPa. The properties were different between specimens N0 and V0, since they were cast on different days.

2.1.2 Experimental results from the specimens containing aggregates

Forced vibration tests were conducted on specimens N0 and BF, as shown in **Figure 1**. During these tests, a white noise signal was applied to the cylinders from the upper face. A portable vibrator was controlled to cover the frequency range of 2000 to 15,000 Hz. The acceleration power spectrum density (PSD) was 0.5 (m/s^2)^2/Hz, and the root mean square (RMS) was 81 m/s^2. The excitation duration was around 5 seconds. Frequency responses were measured with an accelerometer placed on the upper face of the cylinders.

The frequency responses of specimens N0 and BF are shown in **Figure 4**. The resonant frequency, defined in this study as the frequency giving the maximum response amplitude, of specimen N0 was observed as 8720 Hz, whereas that of specimen BF was 10,760 Hz. This is mainly because the dynamic elastic modulus of the glass aggregates was higher than that of the mortar.

Using a parallel model, an equivalent wave speed within composite material containing spherical inclusions can be estimated. The equivalent wave speed c_0 and dynamic elastic modulus E_0 are evaluated from [11]

$$\frac{1}{c_0} = \frac{V_g}{c_g} + \frac{V_m}{c_m} \tag{1}$$

$$c_0 = 2Lf_0 = \sqrt{\frac{E_0}{\rho_0}} \tag{2}$$

where, c_g and c_m are the speeds of sound within glass and mortar respectively, V_g and V_m are the volume ratios of glass and mortar, f_0

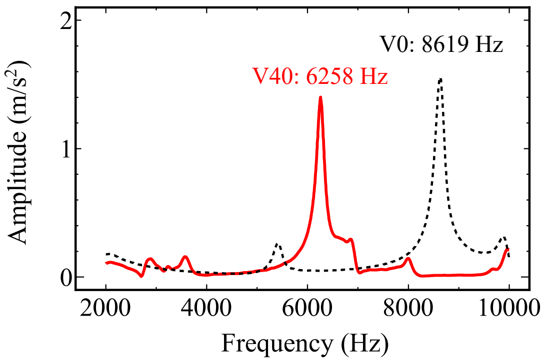

Figure 5: Frequency responses of specimens V0 and V40.

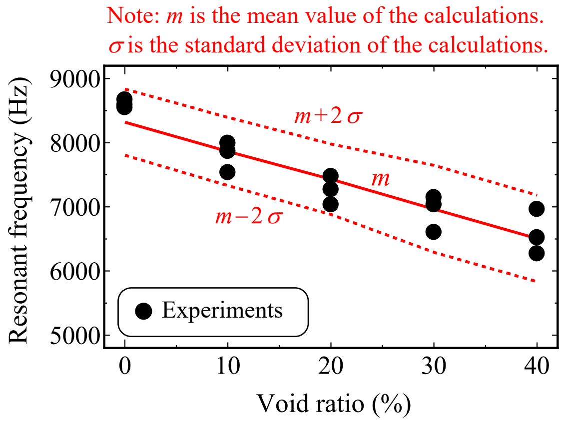

Figure 6: Relationship between resonant frequency and void ratio.

is the resonant frequency, and ρ_0 is the average mass density of composite material. The glass material properties were estimated from the measured frequency f_0 = 10,760 Hz: the speed of sound c_g = 5397 m/s and the dynamic elastic modulus was 71,300 MPa. These values were higher than those of the mortar.

2.1.3 Experimental results from the specimens containing voids

Specimens V0 to V40 were excited with compressive waves in the longitudinal direction using sinusoidal forcing through a frequency sweep of 2000-10,000 Hz. The acceleration amplitude of the vibrator was fixed at 0.5 m/s^2 and the sweep duration was 18 seconds.

The frequency responses of specimens V0 and V40 are shown in **Figure 5**. The resonant frequency of specimen V40 decreased to 6258 Hz from 8619 Hz (specimen V0). The relationship between resonant frequency and void ratio is shown in **Figure 6**. The resonant frequency decreased as the void ratio increased, since the equivalent speed of sound c_0 and dynamic elastic modulus E_0 were lower.

As implied, the inclusions within the mortar can be detected from the resonant frequency measurements.

2.2 Wave propagation analyses

2.2.1 Calculation model

Wave propagation analyses were used to interpret the experimental results. The calculation model, based on a finite difference time domain (FDTD) method [12-14], is shown in **Figure 7**. Based on a staggered grid, the three dimensional wave equations are given as [13]

$$v_x^{n+\frac{1}{2}}\left(i+\frac{1}{2},j,k\right)=v_x^{n-\frac{1}{2}}\left(i+\frac{1}{2},j,k\right)-\frac{\Delta t}{\rho\,\Delta x}\left\{p^n(i+1,j,k)-p^n(i,j,k)\right\} \tag{3}$$

$$v_y^{n+\frac{1}{2}}\left(i,j+\frac{1}{2},k\right)=v_y^{n-\frac{1}{2}}\left(i,j+\frac{1}{2},k\right)-\frac{\Delta t}{\rho\,\Delta y}\left\{p^n(i,j+1,k)-p^n(i,j,k)\right\} \tag{4}$$

$$v_z^{n+\frac{1}{2}}\left(i,j,k+\frac{1}{2}\right)=v_z^{n-\frac{1}{2}}\left(i,j,k+\frac{1}{2}\right)-\frac{\Delta t}{\rho\,\Delta z}\left\{p^n(i,j,k+1)-p^n(i,j,k)\right\} \tag{5}$$

$$\begin{aligned}p^{n+1}(i,j,k)&=p^n(i,j,k)\\&-\rho c^2\frac{\Delta t}{\Delta x}\left\{v_x^{n+\frac{1}{2}}\left(i+\frac{1}{2},j,k\right)-v_x^{n+\frac{1}{2}}\left(i-\frac{1}{2},j,k\right)\right\}\\&-\rho c^2\frac{\Delta t}{\Delta y}\left\{v_y^{n+\frac{1}{2}}\left(i,j+\frac{1}{2},k\right)-v_y^{n+\frac{1}{2}}\left(i,j-\frac{1}{2},k\right)\right\}\\&-\rho c^2\frac{\Delta t}{\Delta z}\left\{v_z^{n+\frac{1}{2}}\left(i,j,k+\frac{1}{2}\right)-v_z^{n+\frac{1}{2}}\left(i,j,k-\frac{1}{2}\right)\right\}\end{aligned} \tag{6}$$

where, c is the speed of sound, ρ is the mass density, p is the sound pressure, v_x, v_y, v_z are the three components of particle velocity, Δx, Δy, Δz are the spatial discretization steps, and Δt is the time discretization step. The indices i, j, k are the spatial points, the index n is the time point.

For specimens N0 and BF, a sound pressure

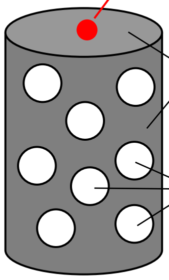

Figure 7: FDTD method applied to the cylinder specimen containing voids.

of white noise over the range of 3000-14,000 Hz was applied, as shown in **Figure 7**. The spatial discretization steps $\Delta x = \Delta y = \Delta z = 2$ mm and the time discretization step $\Delta t = 0.18$ *u*s. Resonant frequency was obtained from a FFT analysis of the response of the sound pressure during an excitation period of $T = 65{,}536 \times \Delta t = 12$ ms.

On the other hand, for specimens V0 to V40, a sound pressure with a frequency sweep of 3000-10,000 Hz was applied. The spatial discretization steps Δx, Δy, Δz were the same as those of specimens N0 and BF, but the time discretization step Δt and excitation period T were changed to 0.30 *u*s and 0.20 ms, respectively, to ensure stability of the analyses.

In the calculations, the material properties were set equal to the experimental values. In specimens V10 to V40, the boundary conditions around the spherical voids were given as $v_x = v_y = v_z = 0$. Influence of shear waves and damping were not considered in Eqs. (3)-(6); they were minimal in affecting the resonant frequency.

As shown in **Figure 3**, in specimen BF, the aggregates were specifically arranged, whereas the spherical voids in specimens V10 to V40 were randomly distributed within the cylinders. The locations of the voids were randomly adjusted in Monte Carlo simulations of 1000 trials. Additionally, the coefficient of variation of the sound speed within mortar c_m was assumed as 3% in these simulations [10].

2.2.2 Calculation results

As shown in **Table 2**, the experimental and calculation results from specimens N0 and BF

Table 2: Resonant frequency of specimens N0 and BF.

Specimen	Resonant frequency (Hz)	
	Experiments*	Calculations
N0	8720	8308
BF	10,740	9918

*Average of three cylinder specimens

were in good agreement. These calculations imply that the influence of wave reflection and scattering on the aggregate surfaces are minor during the standing vibration, where the wavelength was $2L$.

On the other hand, the resonant frequency decreased in the calculations of V0 to V40, as shown in **Figure 6**. The experimental results were included in the range of $m \pm 2\sigma$ with respect to the calculation results, where m and σ are the mean value and coefficient of variation, respectively. In the calculations, the waves diffracted around the voids within the mortar cylinders, resulting in the decrease in resonant frequency as the void ratio increased during the standing vibration.

The use of a numerical simulation proved beneficial in interpreting the experimental results and understanding the wave propagation behavior within the cylinders. It is also valuable for evaluating internal damage conditions within the composite material.

3 EVALUATION OF INTERFACE FRACTURE

In this section, detection of interface fracture within the composite material was examined using the testing and calculation methods. The interface fracture was induced in specimen BF by applying quasi-static load. Two displacement gauges were set beside the cylinders in the vertical direction. A vibration test was conducted on the cylinders (**Figure 1**) taken from a loading machine, at each load step of 20 kN up to the maximum load, as well as each displacement step of 0.1 mm in the post peak region.

From specimens N0 and BF, the relationships between average stress and strain are shown in **Figure 8**. The compressive strengths of specimens N0 and BF were

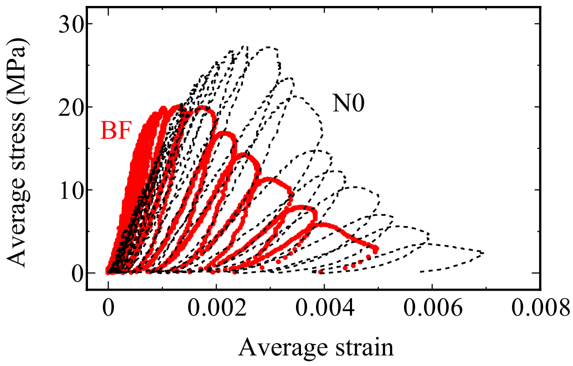

Figure 8: Relationship between stress and strain.

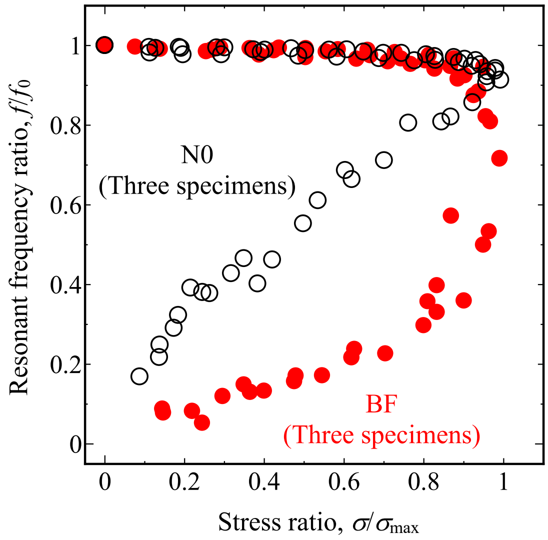

Figure 9: Relationship between resonant frequency and stress.

around 28 and 20 MPa, respectively. The strength of specimen BF was lower, but its stiffness was higher than that of specimen N0, since the aggregates had a higher elastic modulus.

The relationships between resonant frequency and applied stress are given in **Figure 9**, where the stress has been normalized by compressive strength, and the frequency has been normalized by initial value. In specimen N0, the decrease of the resonant frequency was slight until the maximum stress. The frequency ratio decreased to 0.95 at the maximum stress, and then continued to decrease linearly as the stress ratio decreased in the post peak region. It was thought that formation of internal cracks caused a depression in the load capacity of the cylinder before progressing gradually in the post peak region.

On the other hand, the result of the aggregate-containing specimens differed greatly in comparison. In specimen BF, the frequency ratio decreased significantly around the maximum stress to 0.5. From the FDTD analysis, at the point when interface fracture was noted on all aggregate-mortar boundaries, the resonant frequency was calculated as f = 5188 Hz, where the boundary condition was given as $v_x = v_y = v_z = 0$. The calculated frequency ratio f/f_0 was obtained as 0.52, with an initial value f_0 = 9918 Hz, as shown in **Table 2**. The result comparison between the calculations and experiments indicated that most of the interface fracture between the aggregates and mortar transpired up to the maximum stress. After the load tests, still intact glass aggregates were taken from the mortar matrix, as shown in **Figure 10**.

Figure 10: Glass aggregates taken from the mortar matrix.

4 CONCLUSIONS

In this study, forced vibration tests were conducted on model concrete cylinders containing spherical glass aggregates or voids for detecting interface fracture within the composite material. Moreover, wave propagation analyses were used to interpret the experimental results. From these experiments and calculations, the following findings were observed:

1. Using a portable vibrator, the resonant frequency of the cylinders was measured from the standing vibration. The resonant frequency decreased as the amount of internal voids increased. Similar results were also obtained in the specimens exhibiting interface fracture between glass

aggregates and mortar.

2. From the calculations of the specimens containing voids, waves diffracted around the voids during the standing vibration. Diffraction of the waves decreased the resonant frequency. A comparable calculation result was also obtained for the cylinders containing interface fracture, which act as slits (thin voids) on the aggregate-mortar boundaries.
3. The evaluation of internal damage conditions within these composite materials was demonstrated using the testing and calculation methods. In the load tests, internal cracks were relatively stable in the plain mortar cylinders in the vicinity of maximum load, whereas damage of the cylinders containing the glass aggregates developed quickly.

From these findings, this approach is shown to be useful in detecting and quantifying interface fracture and other forms of damage. With further research, it can be applied to designing new composite materials, improving their performance, and inspection and evaluation of aging composite structures.

REFERENCES

[1] Buyukozturk, O. and Hearing, B., 1998. Crack propagation in concrete composites influenced by interface fracture parameters. *Int. J. Solids Struct.* **35**:4055-66.

[2] Kim, H., Wagoner, M.P. and Buttlar, W.G., 2009. Simulation of fracture behavior in asphalt concrete using a heterogeneous cohesive zone discrete element model. *J. Mater. Civ. Eng.* **20(8)**: 552-63.

[3] Landis, E.N. and Bolander, J.E., 2009. Explicit representation of physical processes in concrete fracture. *J. Phys. D Appl. Phys.* **42**:1-17.

[4] Feng, M.Q., Flaviis, F.D. and Kim, Y.J., 2002. Use of microwaves for damage detection of fiber reinforced polymer-wrapped concrete structures. *J. Eng. Mech.* **128(2)**:172-83.

[5] Schickert, M., 2002. Ultrasonic NDE of concrete. *IEEE Ultrasonic Symposium.* **1**:739-48.

[6] Suaris, W. and Fernando, V., 1987. Detection of crack growth in concrete from ultrasonic intensity measurements. *Materials and Structures.* **20**:214-20.

[7] Iyer S.R., Sinha, S.K. and Schokker, A.J., 2005. Ultrasonic C-scan imaging of post-tensioned concrete bridge structures for detection of corrosion and voids. *Comput. Civ. Infrastruct. Eng.* **20**:79-94.

[8] Ahn, E., Kim, H., Sim, S.H., Shin, S.W. and Shin, M., 2017. Principles and applications of ultrasonic-based nondestructive methods for self-healing in cementitious materials. *Materials*. **10**:21-5.

[9] Schubert, F. and Kohler, B., 2008. Ten lectures on impact-echo. *J. Nondestruct Eval.* **27**:5-21.

[10] Naito, H. and Bolander, J.E., 2019. Damage detection method for RC members using local vibration testing. *Engineering Structures*. **178**:361-74.

[11] Schickert, Turnik, G., Kavcic, F. and Turk, G., 2009. Prediction of concrete strength using ultrasonic pulse velocity and artificial neural networks. *Ultrasonics*. **49**:53-60.

[12] Gunsteren, W.F. and Berendsen, H.J.C., 1988. A leap-frog algorithm for stochastic dynamics. Molecular Simulation. **1**:173-85.

[13] Botteldooren, D., 1995. Finite-difference time-domain simulation of low-frequency room acoustic problems. *J. Acoust. Soc. Am.* **98(6)**:3302-8.

[14] Botteldooren D., 2005. Acoustical finite -difference time-domain simulation in a quasi-Cartesian grid. *J. Acoust. Soc. Am.* **95**:2313-9.